Chlorine activated stacking fault removal mechanism in thin film CdTe solar cells: the whole story

Peter Hatton
Loughborough University
Michael Watts
Loughborough University
Ali Abbas
Loughborough University
Tom Fiducia
Loughborough University
John Walls
Loughborough University
Roger Smith
Loughborough University https://orcid.org/0000-0001-8147-431X
Pooja Goddard (p.goddard@lboro.ac.uk)
Loughborough University https://orcid.org/0000-0001-6624-2561

Article

Keywords: Absorber Microstructure, Hole Traps, Tetrahedral Stacking Fault, Cascade Effect, Grain Boundary Saturation

Posted Date: March 17th, 2021

DOI: https://doi.org/10.21203/rs.3.rs-333846/v1

Version of Record: A version of this preprint was published at Nature Communications on August 23rd, 2021. See the published version at https://doi.org/10.1038/s41467-021-25063-y.

Chlorine activated stacking fault removal mechanism in thin film CdTe solar cells: the whole story

Peter Hatton,[1] Michael J. Watts,[2] Ali Abbas,[3] Tom Fiducia,[3] John M. Walls,[3] Roger Smith,[1] and Pooja Goddard*[2]

[1] *Department of Mathematical Sciences, Loughborough University, Loughborough, Leicestershire, UK, LE11 3TU*
[2] *Department of Chemistry, Loughborough University, Loughborough, Leicestershire, UK, LE11 3TU*
[3] *Centre for Renewable Energy Systems Technology (CREST), Loughborough University, Loughborough, Leicestershire, UK, LE11 3TU*

(Dated: March 16, 2021)

The efficiency of as-deposited CdTe solar cells is typically <5 %. An activation process involving the post-treatment of the CdTe surface with cadmium chloride at $\approx 400^\circ$ C improves the absorber microstructure by removing stacking faults, fills the grain boundaries with chlorine and leads to efficiencies of up to $\simeq$ 22 % . Stacking fault removal and improvement in device efficiency are thus correlated but the question of whether this correlation is direct or indirect has to date not been established. Although some types of stacking fault could be hole traps, those most commonly observed are tetrahedral in nature which recent work has shown to be electrically benign.

For the first time, in this paper, we not only explain the passivation responsible for this efficiency increase but crucially elucidate the associated stacking fault removal mechanism. Experimental work shows that as chlorine is added to the system, the stacking faults gradually disappear from the absorber layer upwards to the surface with some grains being fault-free in the intermediate state before full saturation. At saturation chlorine decorates all the grain boundaries and so the effect of chlorine on a model system of a tetrahedral stacking fault bounded by two grain boundaries is investigated using density functional theory (DFT). We find that if the stacking faults between the grain boundaries were to be removed *without* Cl, this would result in an energy increase for the system. Increasing the chlorine concentration in the grain boundaries decreases the energy difference between the faulted and unfaulted system until a cross-over occurs close to the point at which chlorine saturates the grain boundaries. The atomic mechanisms and energy profile for the stacking fault removal is presented. The removal process is via a cascade effect whereby the system energy gradually increases as the fault is sequentially removed until the layers 'snap' into place. The energy barrier for this to occur is easily overcome with the 400° C temperature treatment. Density of States (DOS) plots of the chlorine saturated structures show that defect passivation occurs in the highly reconstructed grain boundaries due to both interstitial and substitutional chorine. Chlorine saturation is shown to 'disconnect' the two sides of the grain boundary avoiding electronic defects which arise from the interaction of dangling bonds across this region. It is thus concluded that the cell efficiency increase observed is due to the electronic effects of chlorine in the grain boundaries and that the observed stacking fault removal is a bi-product of the chlorine grain boundary saturation.

Electricity generated by photovoltaic modules is an important renewable source of power. The importance of solar electricity increases as device efficiencies improve and costs reduce. Although modules based on silicon absorbers dominate the current market, second generation modules based on cadmium telluride (CdTe) are the most important thin film technology with over 25 GW already installed. Recent advances in thin film CdTe devices, notably the inclusion of selenium as an alloy at the front of the cell, has led to a sharp increase in module efficiency [1–3]. However, despite the impressive advances made, the conversion efficiency of thin film CdTe solar has the potential for further significant improvement because performance is still well short of the Shockley-Queisser theoretical limit, due mainly to the Voltage deficit. Further enhancement in device efficiency depends on an improved understanding of how these polycrystalline materials work and in particular how the detailed microstructure affects the electrical performance. In this paper, we report on a detailed investigation into the relationship between conversion efficiency, grain boundary passivation with chlorine and the removal of planar defects.

As-deposited thin film CdTe solar cells have a poor conversion efficiency typically < 5 % unless deposited at unusually high temperatures. A cross-sectional image of an as-deposited device using Transmission Electron Microscopy (TEM) is shown in Figure 1a. The CdTe absorber was deposited by close spaced sublimation (CSS). A notable feature of this image is the high density of stacking faults that appear as parallel lines across individual grains [4]. The stacking faults terminate at grain boundaries on either side of the grain and can be seen both in figure 2 and the high resolution TEM image of figure 3a.

The conversion efficiency of CdTe solar cells is transformed by an activation process [4]. In this process, $CdCl_2$ is deposited on the surface of the device held at a high temperature typically 400 to 430 °C for about 20 minutes. This process is used universally in research laboratories and in CdTe solar module manufacturing. During the process, chlorine rapidly diffuses along the grain boundaries and accumulates both there and at the device junction. The traditional n type 'buffer' layer has been cadmium sulphide (CdS) and in this material the chlorine also diffuses along CdS grain boundaries and then accumulates along the interface with the transparent conductor (Fluorine doped tin oxide (FTO)). It is not observed to penetrate the FTO [5]. The CdS buffer layer in recently improved devices has been replaced with wide-band gap metal-oxides such as magnesium-doped zinc oxide (MZO) to reduce optical absorption [6, 7]. The chlorine does not decorate the MZO grain boundaries to the same extent and the chlorine accumulates mainly at the interface with the CdSeTe absorber. Although the chlorine has been observed in the grain interiors, it is mostly tightly bound to the CdSeTe or CdTe grain boundaries as shown in the TEM/EDX/NanoSIMS image in Figure 1c and d. This tight segregation has been confirmed in computational work which showed that both interstitial and substitutional chlorine atoms were 2 eV and 1 eV more stable at the boundaries, respectively than in the bulk [8].

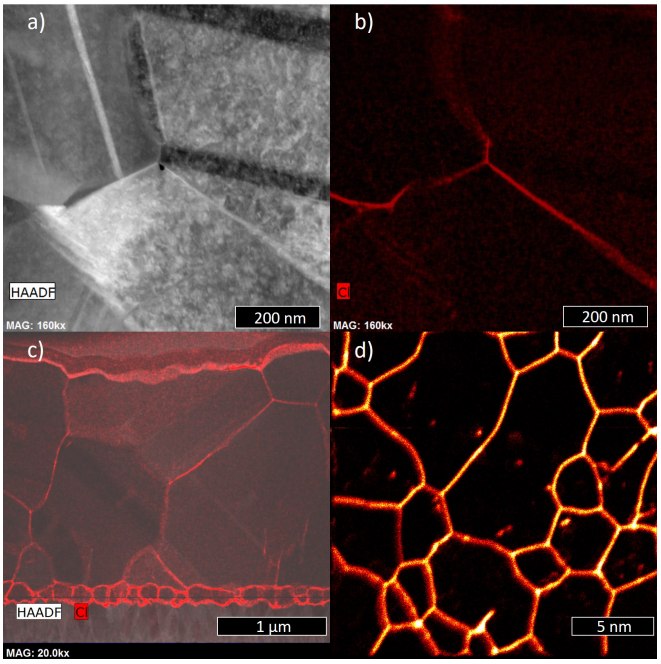

Fig. 1: TEM/EDX/NanoSIMS Images of Cl Treated CdTe. a) TEM image of as-deposited CdTe showing grain boundary/interior structures. b) Same region as in a) with EDX mapping post-treatment CdTe with Cl shown in red; the Cl concentration is high in the grain boundaries compared to bulk. c) Low-resolution TEM image of treated CdTe with EDX mapping of Cl atoms shown to have heavily segregated to the grain boundaries and interfaces. d) $^{35}Cl^-$ signal distribution on the back surface of the as-deposited CdTe absorber showing Cl segregation at grain boundaries after $CdCl_2$ activation.

The chlorine activation process causes a number of changes to the microstructure and improves the electrical performance. The presence of chlorine in the grain boundaries and the removal of stacking faults in the associated grains are signals for the dramatic improvement in cell efficiency. Here we use Density Functional Theory (DFT) to explain how the passivation of the grain boundaries with chlorine and the removal of stacking faults are linked together during the activation process [4]. It has also been observed during a subsequent high temperature anneal without the presence of $CdCl_2$ that the chlorine is removed and the high density of stacking faults return [9]. This is associated with a sharp drop in device efficiency indicating a three-way correlation between the presence of chlorine, stacking faults and device performance.

Figure 2 shows cross-sectional TEM images of a CdTe layer which has undergone partial $CdCl_2$ treatment.

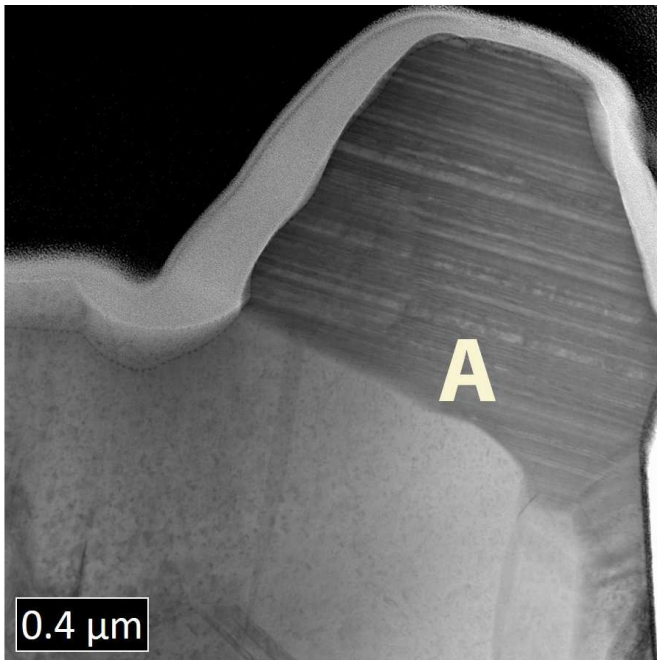

Fig. 2: Low-Resolution Cross-sectional TEM of CdTe Layer. A TEM image of a cross-section of thin film photovoltaic device after a partial activation treatment with cadmium chloride. The grain marked 'A' contains a high density of stacking faults terminating at each end at grain boundaries. Stacking faults have been completely removed in adjacent grains. Stacking fault removal in individual grains is concerted and associated with the density of chlorine located in the grain boundaries.

Stacking faults can be seen as parallel lines running throughout the grain interior. Adjacent grains appear to be in two distinct states of stacking fault removal; either a high density of stacking fault layers can be seen or the grain is clean of these planar defects. These images suggest a stacking fault removal mechanism throughout a grain interior starting at adjacent grain boundaries where there is a local build up of chlorine. This implies that this build up of chlorine at an adjacent grain boundary is key to the removal of stacking faults in each individual grain where the resultant grain structure can be seen in figure 3b after the high temperature chlorine treatment.

The atomic scale mechanisms responsible for grain boundary passivation and stacking fault removal caused by the cadmium chloride treatment are still poorly understood. A DFT study of the electrical properties of stacking faults in CdTe showed that a range of intrinsic and extrinsic stacking fault arrangements are possible and that the high energy types, such as the polytype fault, would act as hole traps [10]. However high resolution TEM experiments have shown that the stacking faults in as-deposited CdTe are predominantly tetrahedral faults [11] which DFT calculations have shown to be electrically benign [12] confirming that the removal of

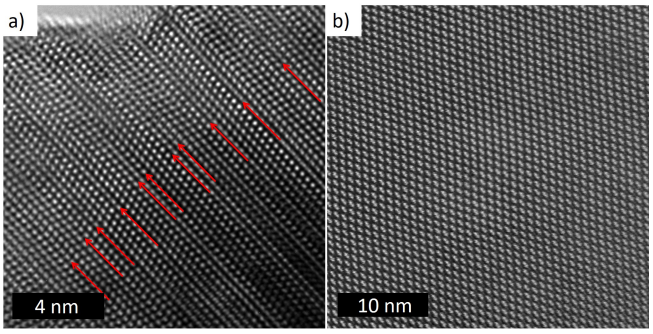

Fig. 3: High-Resolution TEM images of CdTe. HRTEM images of CdTe a) before and b) after $CdCl_2$ treatment showing the existence of a high density of tetrahedral stacking faults (depicted by the red arrows) in as-deposited CdTe which are removed during the high temperature chlorine treatment leaving a purely zinc-blende CdTe structure.

stacking faults is not directly responsible for the efficiency increase.

Nomenclature varies but the most common tetrahedral fault is termed a 'twin stacking fault' in recent experimental work [11, 13, 14] and an 'intrinsic tetrahedral stacking fault' in computational work [12]. A schematic for this type of fault is shown in figure 4. For this fault one layer of atoms is flipped compared to adjacent layers to create a local wurtzite structure in the otherwise zinc-blende lattice. It has been estimated from TEM images that 48 % of layers in as-deposited CdTe have a twin/intrinsic tetrahedral stacking fault structure with the majority of these terminating at grain boundaries [11].

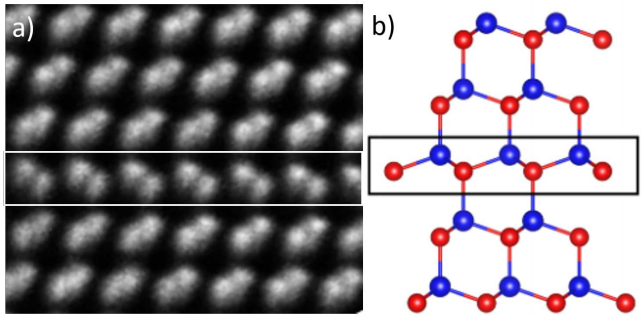

Fig. 4: Intrinsic Tetrahedral/Twin Stacking Fault. a) HRTEM image showing an Intrinsic Tetrahedral/Twin stacking fault [11]. b) Schematic of this type of fault.

The removal of such stacking faults during the chlorine treatment does not contribute to the efficiency increase of the cell [12]. Polytype stacking faults *are* shown to be detrimental to cell performance but these are not likely to form in significant numbers, due to having $\simeq 30$ times the defect energy compared to other stacking fault types [10, 12]. With few observations of polytype faults [11], the

stacking fault removal process via the chlorine treatment is likely to be a mechanical by-product of a separate effect caused by the introduction of chlorine which improves the efficiency.

It has recently been shown that grain boundaries in as-deposited CdTe create cross-boundary Te-Te interactions which cause electronic defects in these regions [8]. These defects can increase electronic recombination causing the low efficiency of the as-deposited cell. This work also showed that if a single chlorine atom were to be present at either interstitial or substitutional sites in an isolated grain boundary structure both would result in defect passivation. If the same were true when many chlorine atoms were present, this would explain the efficiency increase of the CdTe solar cells after the chlorine treatment.

This work is a step change because it considers the effect of chlorine saturation in a model system consisting of a stacking fault terminating at two grain boundaries. The model system consists of an intrinsic tetrahedral stacking fault between two $\Sigma 3$ (112) grain boundaries, types commonly observed in TEM studies, one having a Cd- and the other having a Te-core. Before the addition of chlorine, 154 Cd and Te atoms were arranged in a system approximately $4.57\mathring{A} \times 62.08 \times 18.72\mathring{A}$ with periodic boundary conditions applied in all directions. The $4.57\mathring{A}$ thickness means effectively 1 atomic layer. The structure was then relaxed using DFT to a local minimum energy configuration. The resulting system is shown schematically in figure 5a). It is worth pointing out, that because of the periodic boundaries, the structure shown in figure 5a) really consists of two stacking faults one between the two highlighted grain boundary structures and one that wraps around through the periodic boundaries.

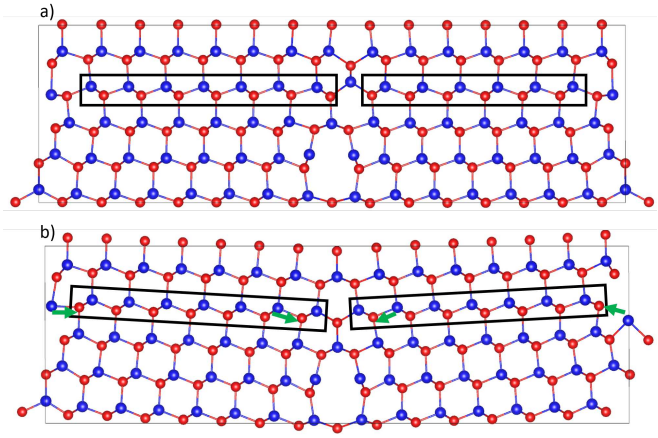

Fig. 5: Cd: Blue, Te: Red. Clean $\Sigma 3$ grain boundary structure. a) Stacking fault structure where the stacking fault layer between two grain boundaries is indicated by the rectangle. b) The same structure with the stacking fault layer removed. The green arrows indicate the Te atom displacements required to transform to the structure shown in a).

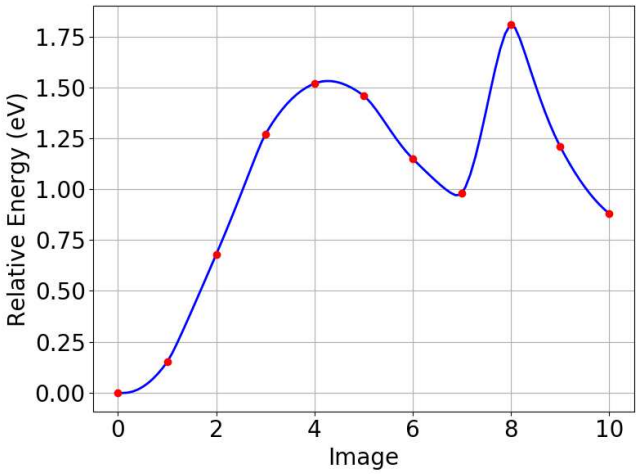

Fig. 6: The energy pathway between figures 5a) to b), determined by the nudged elastic band (NEB) method. The intermediate minimum at image 7 represents the structure in which the stacking fault has been removed in the vicinity of the grain boundary but remains in the grain interior.

Results

Figure 5b shows the same system as in figure 5a but with the stacking fault removed. The relaxed structure shows a small shift in the angle of the layers in the grain interior, indicating strain in the system, but the structures of both grain boundaries are similar with only small changes. The result of this stacking fault removal is a system energy increase of 0.88 eV, implying that in the untreated cell, the system including the stacking fault, is more likely to form.

The energy barrier between the states shown in figure 5 a) and b) has been found using a Nudged Elastic Band (NEB) [15, 16] calculation, the results of which are shown in figure 6. It must be noted that this is before chlorine treatment. The pathway between the two states is found to be through a cascade which begins at both grain boundary cores simultaneously whereby a Te atom close to each boundary switches its bond to the adjacent Cd. The arrows in figure 5b) indicate the Te diffusion direction which initiates the stacking fault removal. The metastable site at image 7 in figure 6 represents the structure where the stacking fault has been removed in the vicinity of the grain boundary but in the middle of the grain interior, the stacking fault remains. A small barrier is required from this point to complete the transition and remove the entire stacking fault.

Since the transition from the system with the stacking fault to the system without involves a barrier of over 1.75 eV and an increase in energy of 0.88 eV, it is unlikely to occur in practice. Furthermore, the reverse barrier of 0.87 eV for re-introducing a stacking fault is much lower than to remove it. Experimentally, it has been shown that stacking faults return when Cl is removed

No. of Cl	Energy Change
0	0.88 eV
9	0.86 eV
12	0.27 eV
13	-0.46 eV
14	-1.02 eV
15	-2.56 eV
16	-2.18 eV
18	-1.54 eV

Table I: System energy change on stacking fault removal with varying amounts of Cl in the Σ3 structure of figures 5a) and b).

through annealing as shown in figure 2. The transition mechanisms without the presence of chlorine suggests it is worth investigating if similar mechanisms exist when chlorine is present in the grain boundaries.

Before considering the stacking fault removal mechanisms themselves the relative stability of the structures shown in figures 5a and b is investigated as chlorine atoms are added to the grain boundaries and the energy difference between the relaxed structures, with and without the stacking fault, is determined.

Table I shows the difference between the systems with and without the stacking faults as the number of chlorine atoms in the grain boundary is increased. With each chlorine concentration, the structure is minimised with and without the stacking fault layer from a variety of starting chlorine positions. The chlorine configurations which resulted in the lowest energy is used and the energy change recorded. This data suggests that increasing the saturation of chlorine in the grain boundaries reduces the energy change on stacking fault removal. The 'switch over' occurs with a total of 13 chlorine atoms in the system but the largest energy decrease is seen with 15 chlorine atoms ($\simeq$ 20 % saturation) in the system which has 6 chlorine atoms in the Cd-core and 9 chlorine atoms in the Te-core. At this point, the grain boundaries are saturated since the addition of further chlorine not only reduces the energy difference but the chlorine atoms move into the grain interior during the relaxation process.

The determination of a pathway between the two states with and without stacking faults is more complex when chlorine was present compared to the case when it was absent. The procedure involved determining intermediate metastable states as suggested in the case without the chlorine and stitching these together piece by piece using the NEB method. This procedure was carried out for the system containing 14 atoms, the NEB calculation for which is shown in figure 7 with an overall barrier of 1.4 eV, easily overcome at 400°.

Images before and after the stacking fault removal with 14 chlorine atoms can be seen in figure 8a) and f), respectively. Large reconstructions have occurred in both cores compared to the clean structures. The grain interiors remain chlorine-free and bulk-like but exhibit the same slight tilting seen with stacking fault removal without chlorine.

Different states along the pathway are also shown in figure 8. The initiation of the stacking fault removal occurs in figure 8b) with the corresponding energies shown in images 0 - 5 of figure 7. A Te atom close to the Cd-core breaks its bond with an adjacent Cd and moves to an interstitial position highlighted in the black rectangle.

From this structure, a Te cascade is initiated propagating into the grain interior where each Te atom in the stacking fault layer switches the Cd it is bonded to. The result of the first of these movements can be seen in figure 8c). The stacking fault has only been removed in the region indicated by the rectangle but remains in the rest of the grain interior. Remarkably, this structure is similar to one that has been imaged experimentally by Chen Li *et al.* [17] finding that mid-grain dislocations create a mid-grain stacking fault terminating at Cd/Te dislocations. However, they were not able to elucidate the whole removal mechanism from this image alone nor do they have information on the saturation of chlorine that triggers this removal mechanism. In our example, the role of the Te dislocation is played by the Te-core grain boundary and a Cd dislocation has been created within the grain, indicated by the blue circle.

Subsequent barriers from image 15 to image 25 represent the cascading removal of the stacking fault via Te diffusing along the stacking fault layer. This mechanism has also been imaged by Chen Li *et al.* [17], showing the Cd dislocation approaching the Te dislocation and therefore the shortening of the stacking fault structure via Te diffusion until the dislocations annihilate creating a clean structure. Figure 8d) shows the result of this cascading Te mechanism, each transition having a small $\simeq$ 0.4 eV energy barrier. When the cascade reaches the middle of the grain interior the system energy plateaus. The process proceeds along the stacking fault layer until the inner stacking fault between the grain boundaries is removed. This occurs at image 25 of figure 7 with the structure shown in figure 8d.

At image 25, the 'wrap-around' stacking fault still remains but is subsequently removed by a similar Te cascade process that begins at the Cd and Te cores simultaneously. The metastable state at image 30, figure 8e), represents the 'wrap-around' stacking fault having been

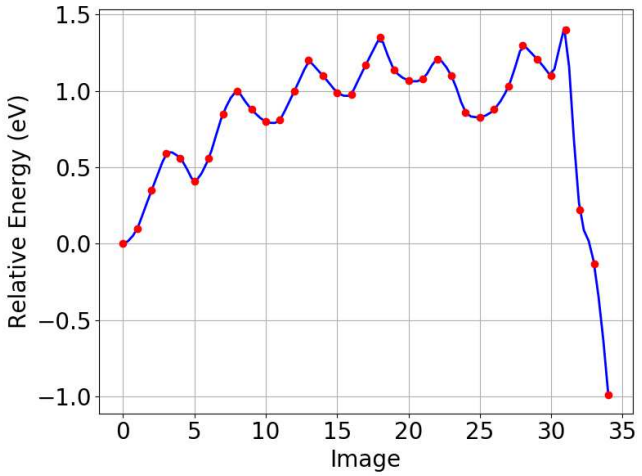

Fig. 7: NEB calculation of the stacking fault removal process with 14 Cl. The change in energy along the pathway from figure 8a) to f). Images 0 - 25 represent a Te cascade starting from the Cd-core and completely removing the stacking fault between the two cores. This mechanism can be seen in figure 8a) to d). Images 25-34 represent the removal of the 'wrap-around' stacking fault through the cell's periodic boundaries. The mechanism here is shown in figure 8d) to f) with a atomic mechanism similar to the 0 Cl case where the stacking fault layer is removed first in the vicinity of both grain boundaries simultaneously then in the grain interior.

removed in the vicinity of the grain boundaries but remaining in the grain interior further from the boundaries, indicated by the rectangle, similar to the mechanism with no chlorine. This structure creates a Cd- and Te- dislocation core shown in blue and red circles, respectively. This structure again is similar to one identified experimentally by Chen Li *et al.* [17] who saw this structure annihilate via the same Te cascade mechanism under the effect of the scanning beam used for atomic imaging, but not due to chlorine saturation. From the structure in 8e) we estimate that the overall barrier required to complete this annihilation is 0.3 eV, shown in figure 7 images 30 - 34, which would be easily overcome at room temperature. The resultant structure can be seen in 8f).

The pathway suggested above will allow for complete removal of the stacking fault in the system and clearly other pathways may be possible but due to large structural shifts in the model and the computational expense involved in searching for these pathways this has not been considered further.

In recent experimental and modelling studies, chlorine-free CdTe grain boundaries, without stacking faults in the adjacent grain interior, have been shown to contain electronic defects which increase electronic recombination due to mid-band-gap defects [18, 19]. This work focussed on doping Te grain boundary sites with substitutional Cl to passivate these electronic defects. However, it has been recently shown that Cl interstitials will also be present at the grain boundaries through segregation calculations and are necessary to passivate fully electronic defects in these regions [8]. These calculations were carried out in a cell containing 136 Atoms in a system 9.14Å × 46.3Å × 11.25Å, i.e. double the thickness of our model. The passivation required 3 carefully placed chlorine atoms, aimed at blocking 'cross-boundary' interactions between Te atoms, to passivate fully these defects. This suggests that a similar passivation effect might occur with grain boundaries that are saturated with chlorine.

The Density of States (DOS) plot of the stacking fault structure shown in figure 5 is shown in figure 9(a). Several defects are present in the band gap of the structure. The most damaging to cell efficiency would be the defect furthest from the Valence Band Minimum (VBM) between -0.4 eV and 0 eV which is most likely to undergo Shockley-Reed-Hall recombination [20]. There are also defects close to the VBM which are responsible for the flat region extending from the VBM at $\simeq$ -0.6 eV. These defects in the structure with the stacking fault are similar in nature to the defects found without the stacking fault layer and no Cl present [8] with small differences seen in the intensity of some defects most likely due to the 'thinner' model.

Figure 10 shows the physical locations of the electronic defects, concentrated as expected, at the grain boundaries. The defect in figure 10(a) is responsible for the flat region extending from the VBM at $\simeq$ -0.6 eV and is caused by the 'cross-boundary' Te-Te interaction in the Cd-core. Since the stacking fault layer is above the Cd-core structure, the stacking of this layer does not impact the structure of the Cd-core. It is thus expected that this defect will be present regardless of the stacking fault existence. An identical defect was also found in a structure without the stacking fault [8]. Figures 10(b) & (c) are the defects responsible for the region between -0.4 eV and 0 eV in the DOS and both originate in the Te-core. The defect in figure 10(b) is concentrated on the 'cross boundary' Te-Te interaction at the top of the Te-core and this defect is accompanied by the Te at the bottom of the Te-core in figure 10(c) which, while being correctly coordinated, has non-standard bond angles with two adjacent Cd atoms.

The physical location of these Te-core defects are different to those found without the stacking fault layer [8], but the overall conclusion of 'cross-boundary' interactions invoking electronic defects at the grain boundaries which cause defects in the band-gap of the cell is the same.

The DOS plot for the model system with 14 chlorine atoms in the grain boundary and with the stacking fault removed is shown in figure 9(b). This shows clear evidence of the chlorine passivation. The flat defect extending from the VBM due to 'cross-boundary' Te-Te

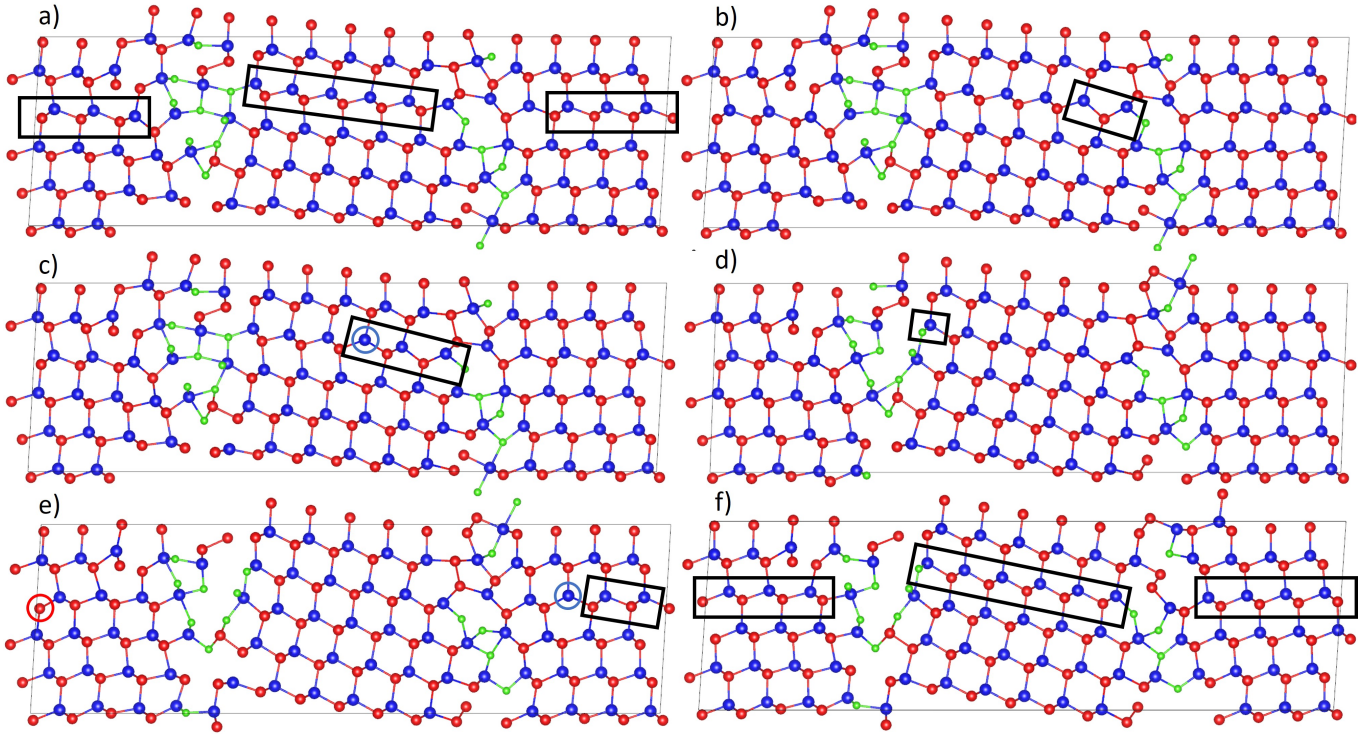

Fig. 8: Atomic Mechanism of Stacking Fault Removal with Cl Saturated Grain Boundaries Cd: Blue, Te: Red, Cl: Green. The energy profile for this mechanism is given in 7. a) (Image 0) Lowest energy stacking fault structure with 14 Cl; the stacking fault layer is indicated by the rectangles. b) (Image 5) The removal is initiated by a Te atom moving to an interstitial position with a 0.6 eV barrier shown in the rectangle. c) (Image 10) The Te cascade has advanced by another step into the grain interior with a 0.6 eV energy barrier. d) (Image 25) The Te cascade has completed the stacking fault removal between the grain boundaries with energy barriers of $\simeq$ 0.4 eV. e) (Image 30) The remaining 'wrap-around' stacking fault is removed in the vicinity of both grain boundary cores simultaneously with 0.6 eV barrier. f) (Image 34) The stacking fault is fully removed resulting in 2.1 eV energy decrease from previous metastable state and a 1 eV energy decrease from the original faulted structure.

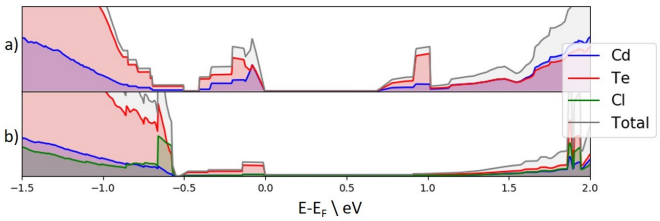

Fig. 9: Normalised DOS Grain Boundary Structure with Varying Cl Concentration. Normalised DOS plot of (a) the clean Σ3 (112) grain boundary structure containing a stacking fault layer and (b) Σ3 (112) grain boundary structure containing 14 Cl without a stacking fault.

interaction in the Cd-core has been removed and there is a significant reduction in the intensity of the main mid-gap defect but with some defect remaining. Analysis shows that all identified defects in figure 10 have been removed and the remaining portion of the mid-gap defect is the result of Te 'noise' throughout the structure related to the single atomic layer thickness necessary for the computationally expensive NEB calculations. We also see a reduction of bands at the edge of the CBM also contributing to the non-defective band gap that would explain the the increased efficiency post $CdCl_2$ treatment.

Conclusion

In this paper, we report for the first time the full mechanism by which stacking fault removal occurs when CdTe solar cells are treated with chlorine. This occurs through a Te cascade mechanism that is triggered when the grain boundaries are saturated by chlorine. The process is demonstrated experimentally through high resolution electron microscopy and nanoSIMS images which clearly show the grain boundaries decorated with chlorine after the stacking fault removal. It is further shown that the grain boundaries saturated by both interstitial and substitutional chlorine remove defects in the band gap. Therefore concluding that the stacking fault removal is a bi-product of the chlorine treatment and that the improved cell efficiency observed after the treatment is due

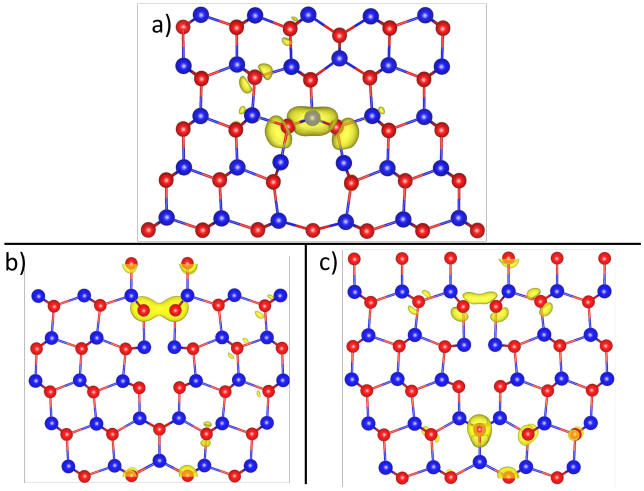

Fig. 10: Partial Charges at the Grain Boundaries with a Stacking Fault Layer Present. (a) 'Cross-boundary' Te-Te interaction in the Cd-core responsible for the defect level at $\simeq$ -0.6 eV in figure 9. (b) 'Cross-boundary' Te-Te interaction in the Te-core partially responsible for the defect level between -0.6 eV and 0 eV in figure 9. (c) Te defect caused by a non-standard Cd bond angle at the bottom of the Te-core partially responsible for the defect level between -0.6 eV and 0 eV in figure 9.

to electronic defect suppression in the grain boundaries, solving the mystery of why and how chlorine is so effective in improving the CdTe cell efficiency. The removal of stacking faults is a useful but indirect, indicator that chlorine in the grain boundary has reached a sufficient concentration to passivate otherwise harmful defects.

Method

To keep the structures size to a minimum for NEB and minimisation operations, only a single CdTe unit thickness is used for the cell depth. The system size measures 4.58 × 61.97 × 18.73 Å with a grain width of 31 Å and contains 154 atoms. The cell length was systematically increased until the defect formation energy of chlorine plateaued in the centre to give a bulk-like environment for the defect. A 4×1×2 k-point grid is used with a 300 eV plane wave basis set cut off for all DFT simulations of this cell which were done using VASP [21]. NEB calculations used the modified solid state climbing image NEB [16, 22, 23] alongside the double-nudging method introduced by Wales *et al.* [24]. The size of the system was chosen so as to contain enough atoms that the effect of chlorine saturation in the grain boundaries and stacking fault removal mechanisms could be observed, without the necessity to use excessive amounts of computational resources. Structures were relaxed until the forces on all atoms converged to < 0.01 eV/Å. DFT calculations were carried out using the PBEsol functional which has been used previously for CdTe systems [8, 12, 25]. A study of chlorine's effects on grain boundaries at the hybrid DFT level of theory is required to confirm and improve understanding of passivation mechanisms; static calculations with 4 × 1 × 2 k-point grids were used.

[1] First Solar, "First solar achieves yet another cell conversion efficiency world record," (2016), available: https://investor.firstsolar.com/news/press-release-details/2016/First-Solar-Achieves-Yet-Another-Cell-Conversion-Efficiency-World-Record/ [Accessed: 28 - Jan - 2021].

[2] A. H. Munshi, J. Kephart, A. Abbas, J. Raguse, J. Beaudry, K. Barth, J. Sites, J. Walls, and W. Sampath, IEEE Journal of Photovoltaics **8**, 310 (2018).

[3] T. A. M. Fiducia, B. G. Mendis, K. Li, C. R. M. Grovenor, A. H. Munshi, K. Barth, W. S. Sampath, L. D. Wright, A. Abbas, J. W. Bowers, and J. M. Walls, Nature Energy **4**, 504 (2019).

[4] A. Abbas, G. D. West, J. W. Bowers, P. Isherwood, P. M. Kaminski, B. Maniscalco, P. Rowley, J. M. Walls, K. Barricklow, W. S. Sampath, and K. L. Barth, IEEE 38th Photovoltaic Specialists Conference (PVSC) (2012).

[5] A. Abbas, P. Kaminski, G. West, K. Barth, W. Sampath, J. Bowers, and J. Walls, MRS Proceedings **1738**, 7 (2015).

[6] A. H. Munshi, J. M. Kephart, A. Abbas, T. M. Shimpi, K. L. Barth, J. M. Walls, and W. S. Sampath, Solar Energy Materials and Solar Cells **176**, 9 (2018).

[7] F. Bittau, C. Potamialis, M. Togay, A. Abbas, P. J. Isherwood, J. W. Bowers, and J. M. Walls, Solar Energy Materials and Solar Cells **187**, 15 (2018).

[8] M. Watts, P. Hatton, R. Smith, T. Fiducia, A. Abbas, R. Greenhalgh, J. M. Walls, and P. Goddard, Physical Review Materials (2021).

[9] A. Abbas, D. Swanson, A. Munshi, K. L. Barth, W. S. Sampath, G. D. West, J. W. Bowers, P. M. Kaminski, and J. M. Walls, 2015 IEEE 42nd Photovoltaic Specialist Conference, PVSC (2015).

[10] S. Yoo, K. T. Butler, A. Soon, A. Abbas, J. M. Walls, and A. Walsh, Applied Physics Letters **105**, 062104 (2014).

[11] T. Fiducia, A. Abbas, K. Barth, W. Sampath, and M. Walls, in *2016 IEEE 43rd Photovoltaic Specialists Conference (PVSC)* (2016).

[12] M. J. Watts, S. R. Yeandel, R. Smith, J. Michael Walls, and P. M. Panchmatia, 2018 IEEE 7th World Conference on Photovoltaic Energy Conversion (WCPEC) (A Joint Conference of 45th IEEE PVSC, 28th PVSEC 34th EU PVSEC) (2018).

[13] T. Paulauskas, C. Buurma, E. Colegrove, Z. Guo, S. Sivananthan, M. K. Y. Chan, and R. F. Klie, Applied Physics Letters **105**, 071910 (2014).

[14] C. Li, J. Poplawsky, Y. Wu, A. Lupini, A. Mouti, D. Leonard, N. Paudel, K. Jones, W. Yin, M. Al-Jassim, Y. Yan, and S. Pennycook, Ultramicroscopy **134**, 113 (2013).

[15] D. Sheppard, R. Terrell, and G. Henkelman, The Journal

of Chemical Physics **128** (2008).
[16] G. Henkelman, B. P. Uberuaga, and H. Jónsson, The Journal of Chemical Physics **113**, 9901 (2000).
[17] C. Li, Y. Wu, T. Pennycook, A. Lupini, D. Leonard, W. Yin, N. Paudel, M. Al-Jassim, Y. Yan, and S. Pennycook, Physical review letters **111**, 096403 (2013).
[18] J. D. Major, M. A. Turkestani, L. Bowen, M. Brossard, C. Li, P. Lagoudakis, S. J. Pennycook, L. J. Phillips, R. E. Treharne, and K. Durose, Nature communications. **7**, 13231 (2016).
[19] C. Li, Y. Wu, J. Poplawsky, T. J. Pennycook, N. Paudel, W. Yin, S. J. Haigh, M. P. Oxley, A. R. Lupini, M. Al-Jassim, S. J. Pennycook, and Y. Yan, Phys. Rev. Lett. **112**, 156103 (2014).
[20] W. Shockley and W. T. Read, Physical Review **87**, 835 (1952).
[21] G. Kresse and J. Furthmüller, Computational Materials Science **6**, 15 (1996).
[22] G. Henkelman and H. Jónsson, The Journal of Chemical Physics **113**, 9978 (2000).
[23] D. Sheppard, P. Xiao, W. Chemelewski, D. D. Johnson, and G. Henkelman, The Journal of Chemical Physics **136**, 074103 (2012).
[24] S. A. Trygubenko and D. J. Wales, The Journal of Chemical Physics **120**, 2082 (2004).
[25] M. J. Watts, T. A. M. Fiducia, B. Sanyal, R. Smith, J. M. Walls, and P. Goddard, Journal of Physics: Condensed Matter **32**, 125702 (2019).

Figures

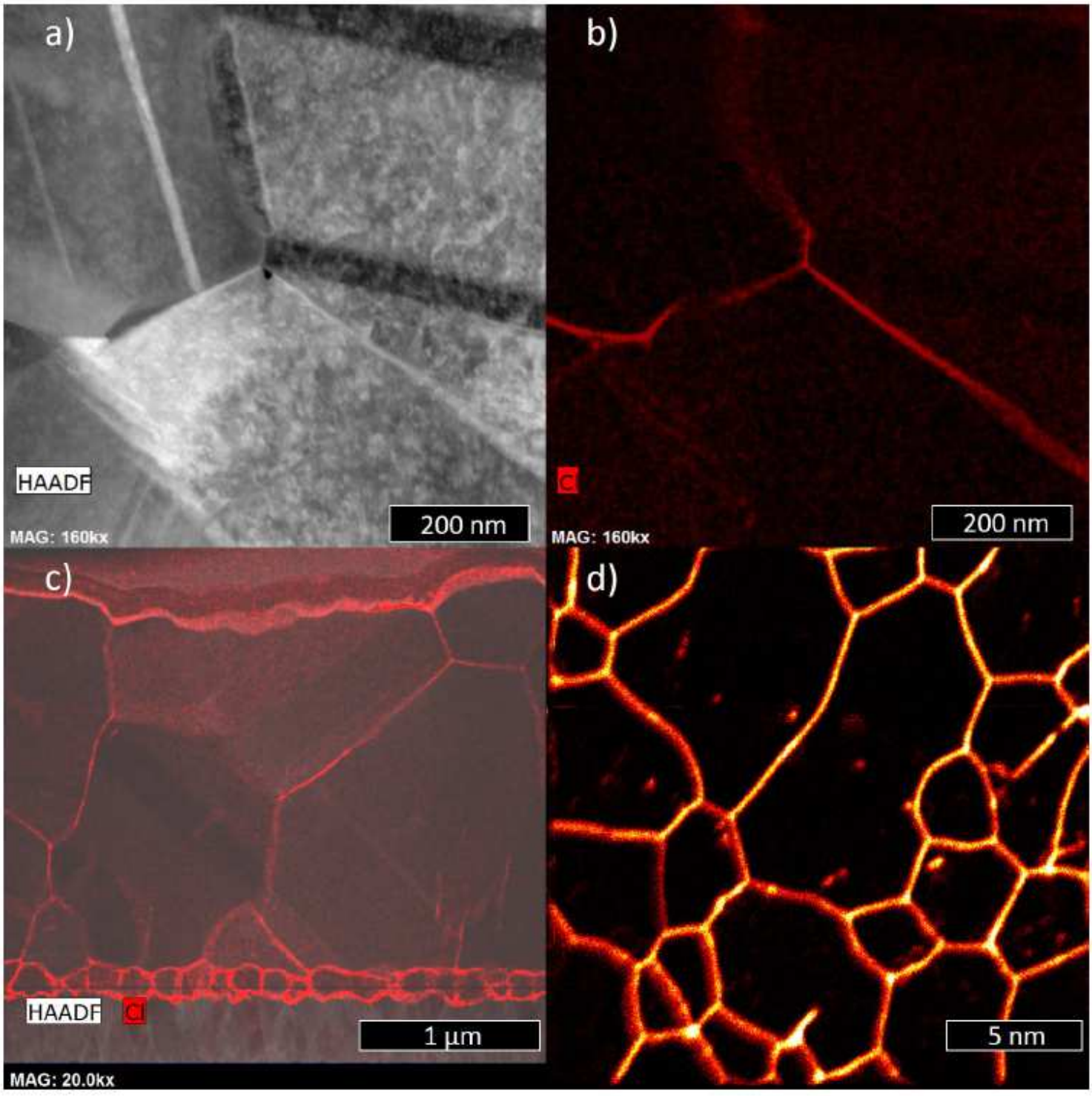

Figure 1

TEM/EDX/NanoSIMS Images of Cl Treated CdTe. a) TEM image of as-deposited CdTe showing grain boundary/interior structures. b) Same region as in a) with EDX mapping post-treatment CdTe with Cl shown in red; the Cl concentration is high in the grain boundaries compared to bulk. c) Low-resolution TEM image of treated CdTe with EDX mapping of Cl atoms shown to have heavily segregated to the grain

boundaries and interfaces. d) 35Cl− signal distribution on the back surface of the as-deposited CdTe absorber showing Cl segregation at grain boundaries after CdCl2 activation.

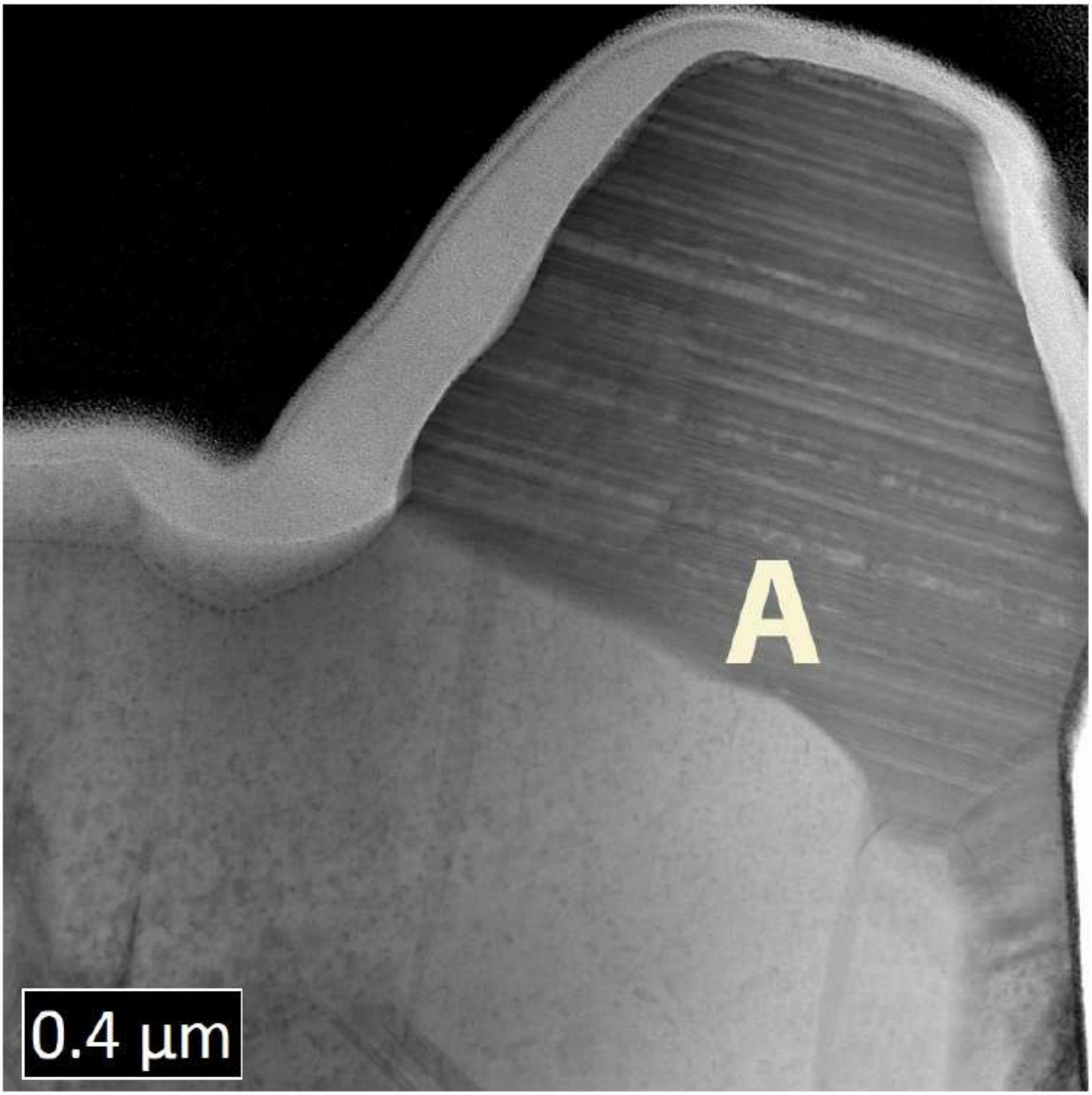

Figure 2

Low-Resolution Cross-sectional TEM of CdTe Layer. A TEM image of a cross-section of thin film photovoltaic device after a partial activation treatment with cadmium chloride. The grain marked ‘A’ contains a high density of stacking faults terminating at each end at grain boundaries. Stacking faults

have been completely removed in adjacent grains. Stacking fault removal in individual grains is concerted and associated with the density of chlorine located in the grain boundaries.

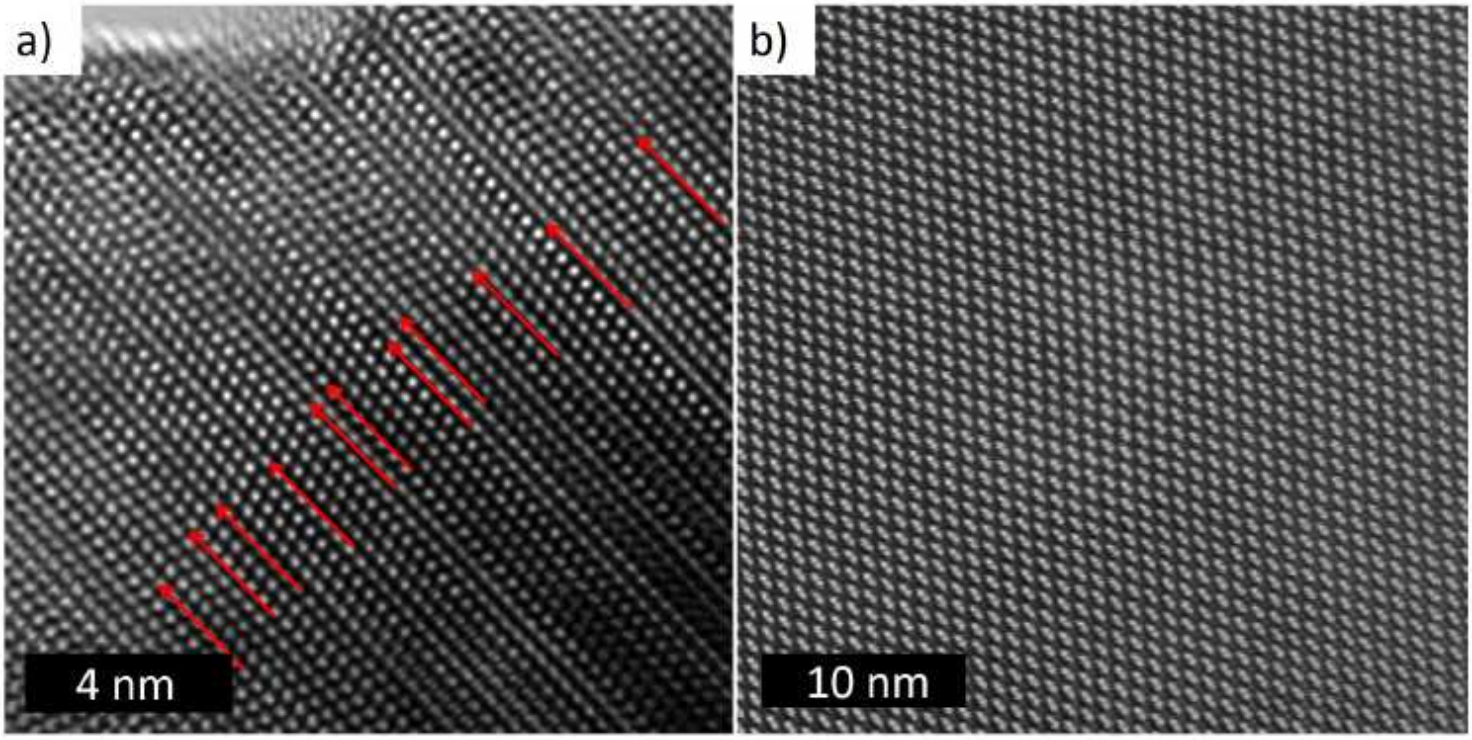

Figure 3

High-Resolution TEM images of CdTe. HRTEM images of CdTe a) before and b) after CdCl2 treatment showing the existence of a high density of tetrahedral stacking faults (depicted by the red arrows) in as-deposited CdTe which are removed during the high temperature chlorine treatment leaving a purely zinc-blende CdTe structure.

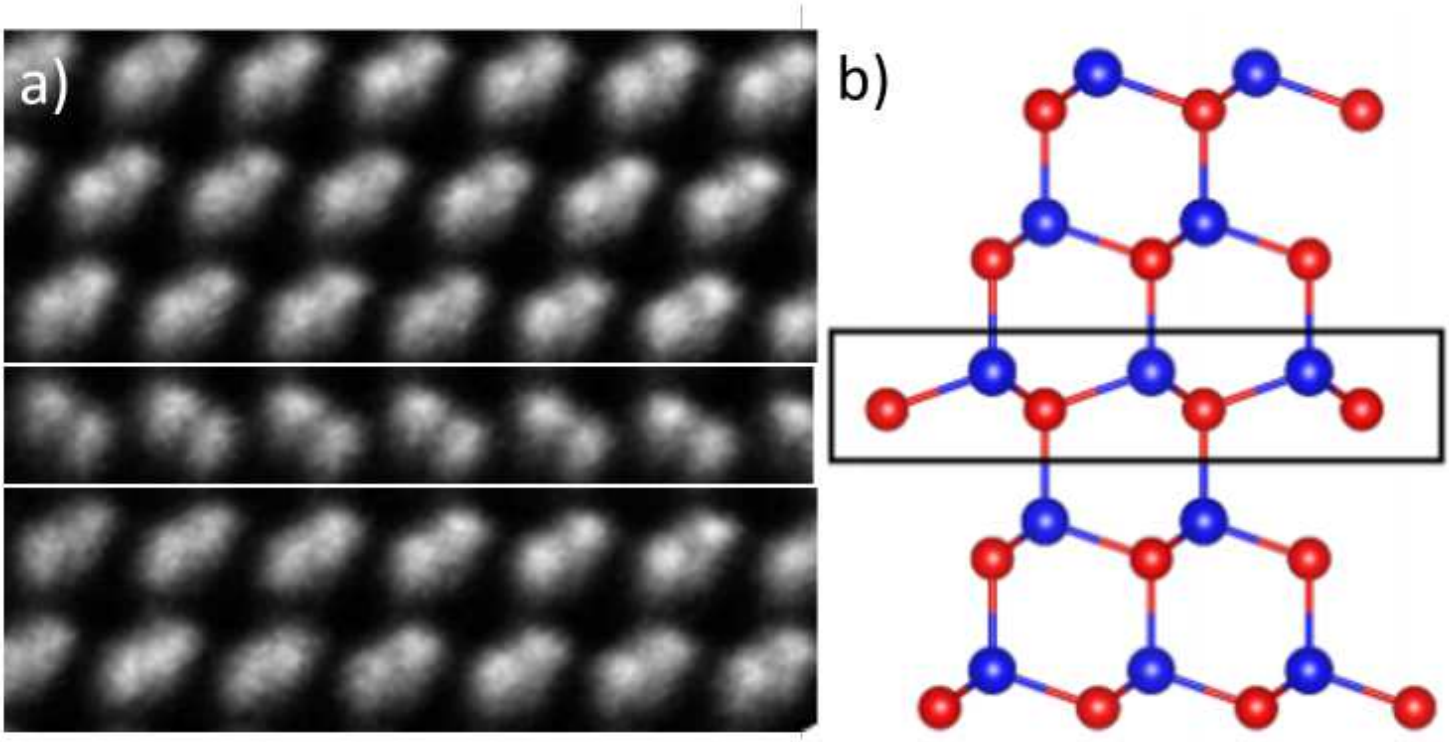

Figure 4

Intrinsic Tetrahedral/Twin Stacking Fault. a) HRTEM image showing an Intrinsic Tetrahedral/Twin stacking fault [11]. b) Schematic of this type of fault.

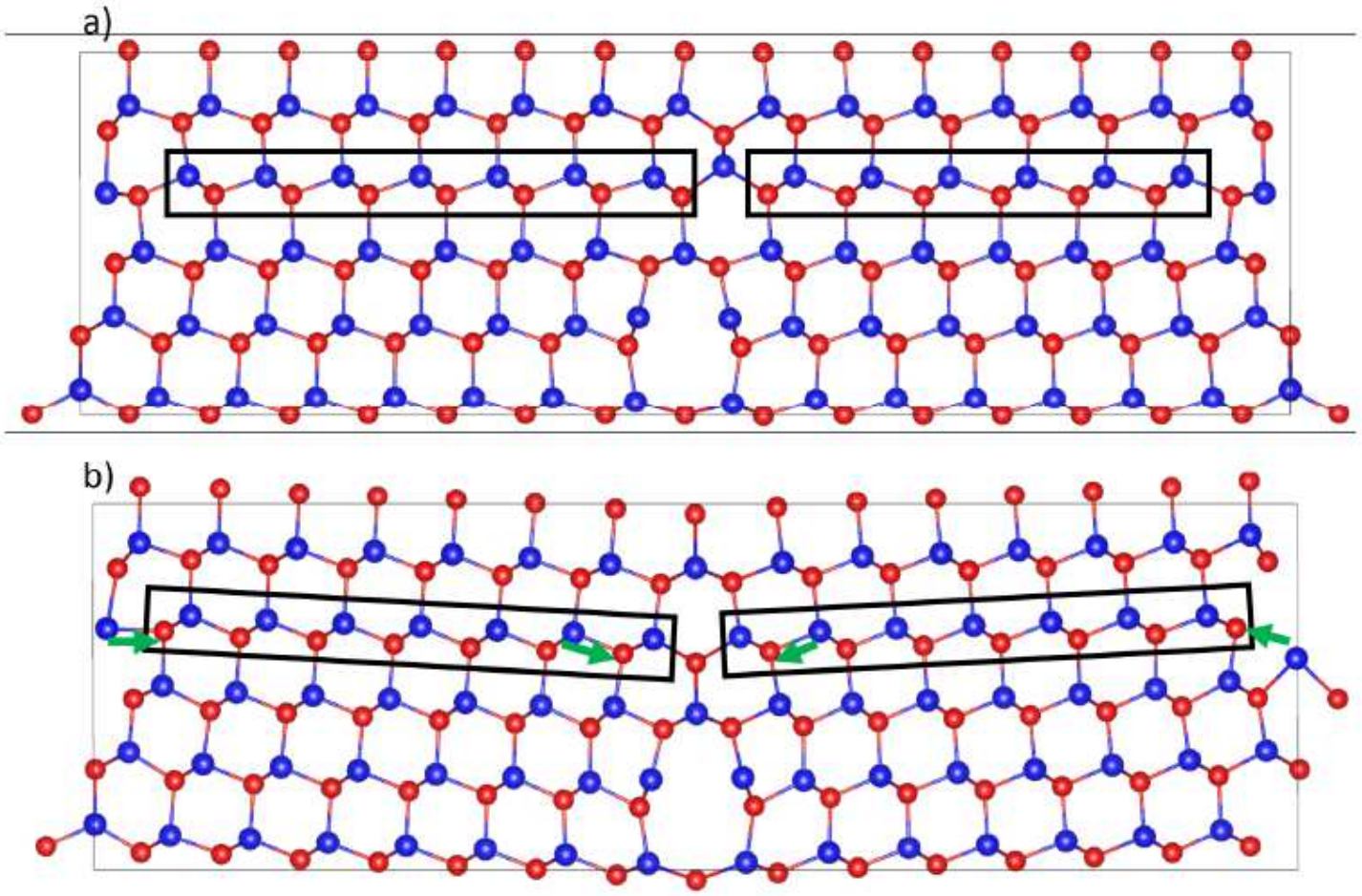

Figure 5

Cd: Blue, Te: Red. Clean Σ3 grain boundary structure. a) Stacking fault structure where the stacking fault layer between two grain boundaries is indicated by the rectangle. b) The same structure with the stacking fault layer removed. The green arrows indicate the Te atom displacements required to transform to the structure shown in a).

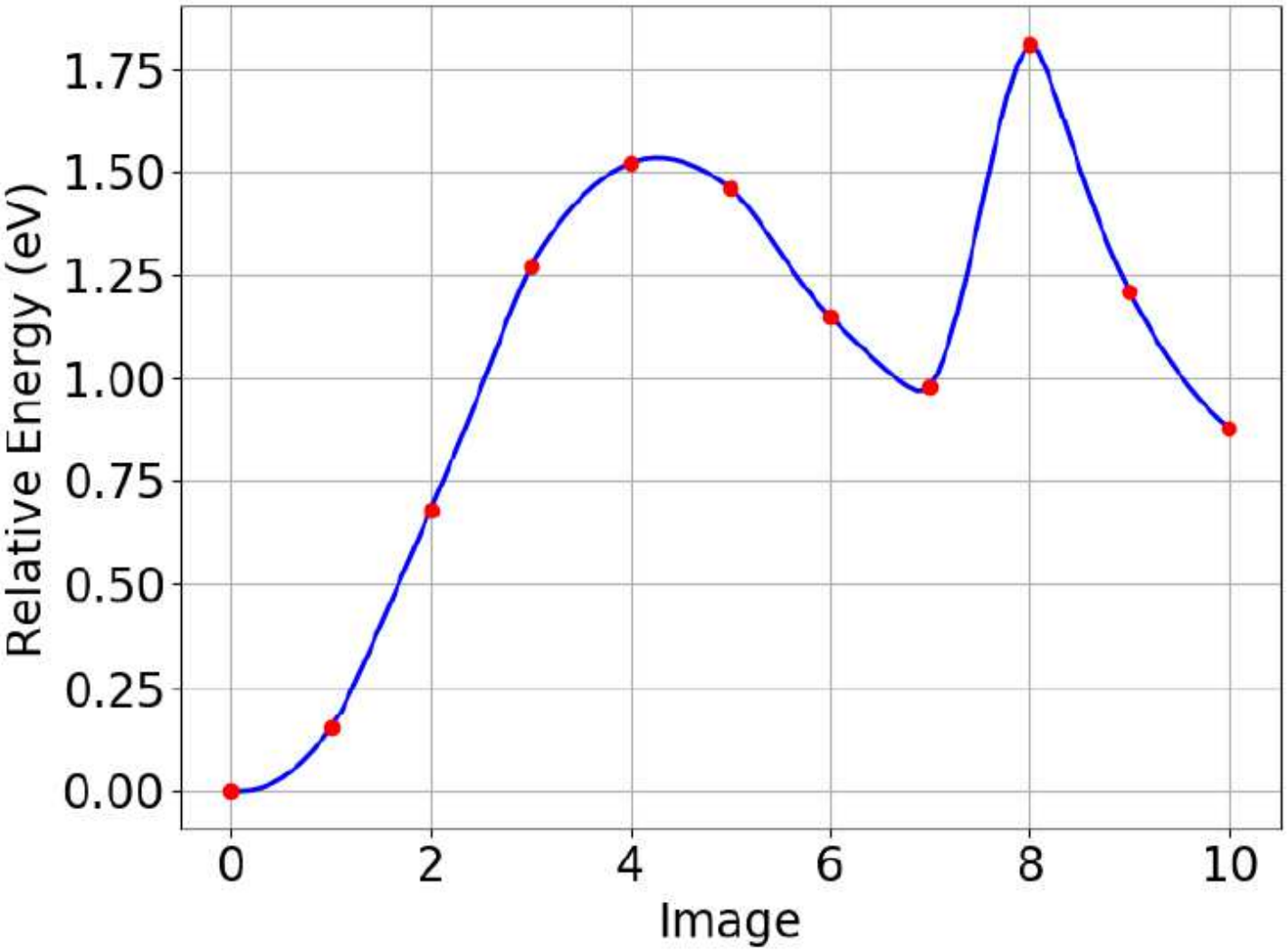

Figure 6

The energy pathway between figures 5a) to b), determined by the nudged elastic band (NEB) method. The intermediate minimum at image 7 represents the structure in which the stacking fault has been removed in the vicinity of the grain boundary but remains in the grain interior.

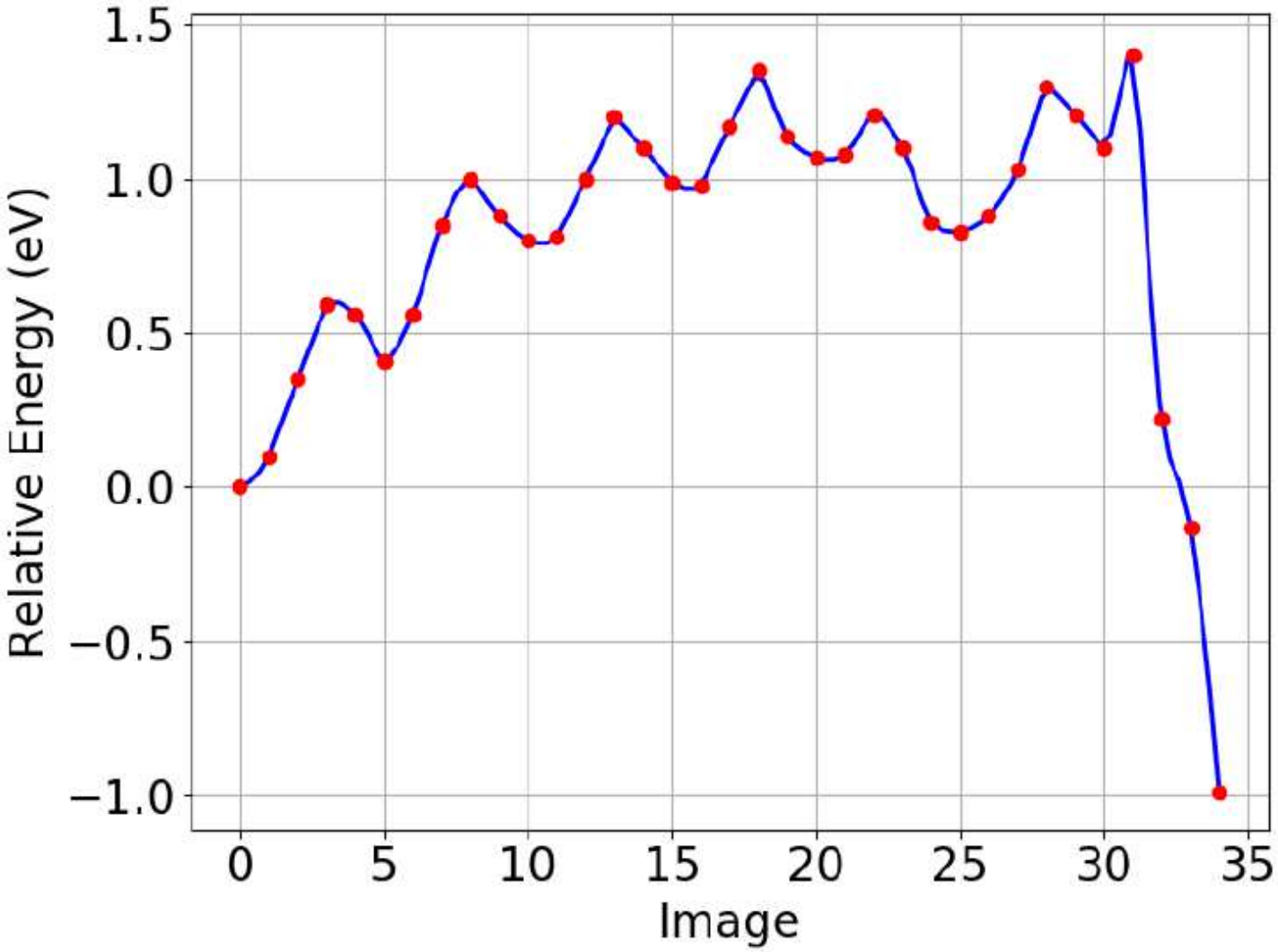

Figure 7

NEB calculation of the stacking fault removal process with 14 Cl. The change in energy along the pathway from figure 8a) to f). Images 0 - 25 represent a Te cascade starting from the Cd-core and completely removing the stacking fault between the two cores. This mechanism can be seen in figure 8a) to d). Images 25-34 represent the removal of the ‘wrap-around’ stacking fault through the cell’s periodic boundaries. The mechanism here is shown in figure 8d) to f) with a atomic mechanism similar to the 0 Cl case where the stacking fault layer is removed first in the vicinity of both grain boundaries simultaneously then in the grain interior.

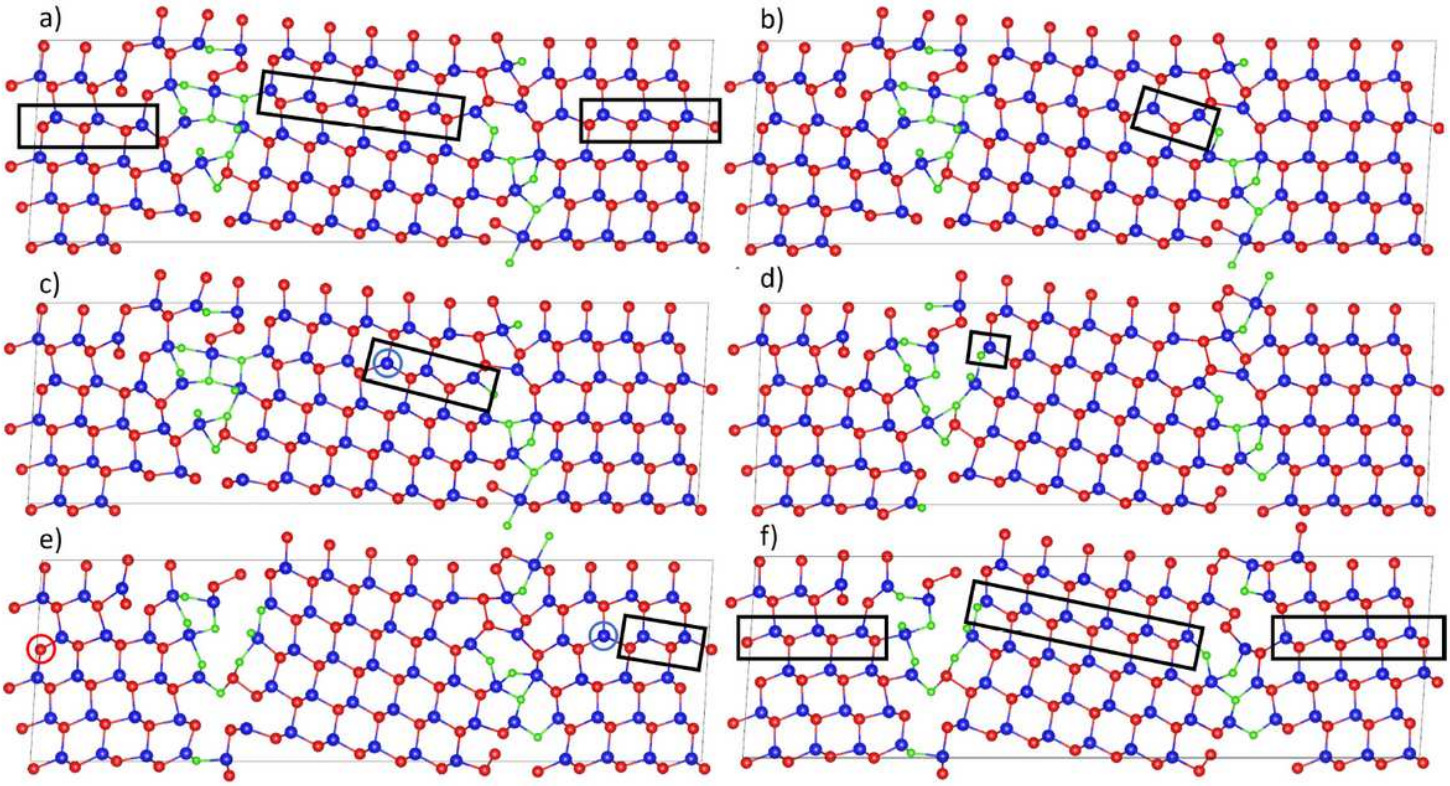

Figure 8

Atomic Mechanism of Stacking Fault Removal with Cl Saturated Grain Boundaries Cd: Blue, Te: Red, Cl: Green. The energy profile for this mechanism is given in 7. a) (Image 0) Lowest energy stacking fault structure with 14 Cl; the stacking fault layer is indicated by the rectangles. b) (Image 5) The removal is initiated by a Te atom moving to an interstitial position with a 0.6 eV barrier shown in the rectangle. c) (Image 10) The Te cascade has advanced by another step into the grain interior with a 0.6 eV energy barrier. d) (Image 25) The Te cascade has completed the stacking fault removal between the grain boundaries with energy barriers of 0.4 eV. e)(Image 30) The remaining ‘wrap-around’ stacking fault is removed in the vicinity of both grain boundary cores simultaneously with 0.6 eV barrier. f) (Image 34) The stacking fault is fully removed resulting in 2.1 eV energy decrease from previous metastable state and a 1 eV energy decrease from the original faulted structure.

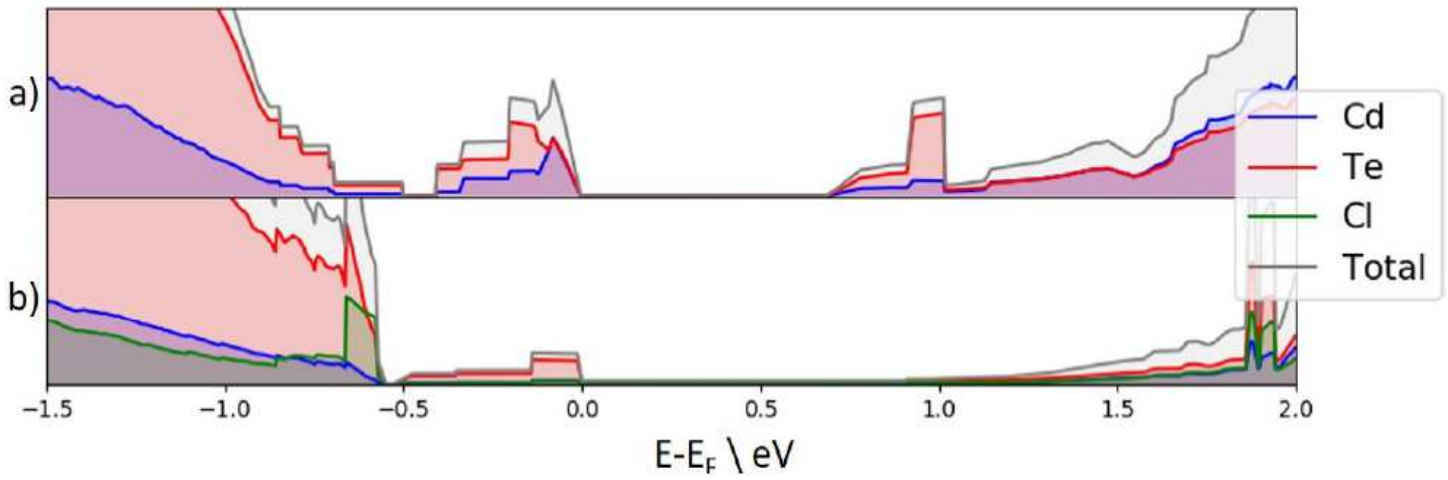

Figure 9

Normalised DOS Grain Boundary Structure with Varying Cl Concentration. Normalised DOS plot of (a) the clean Σ3 (112) grain boundary structure containing a stacking fault layer and (b) Σ3 (112) grain boundary structure containing 14 Cl without a stacking fault.

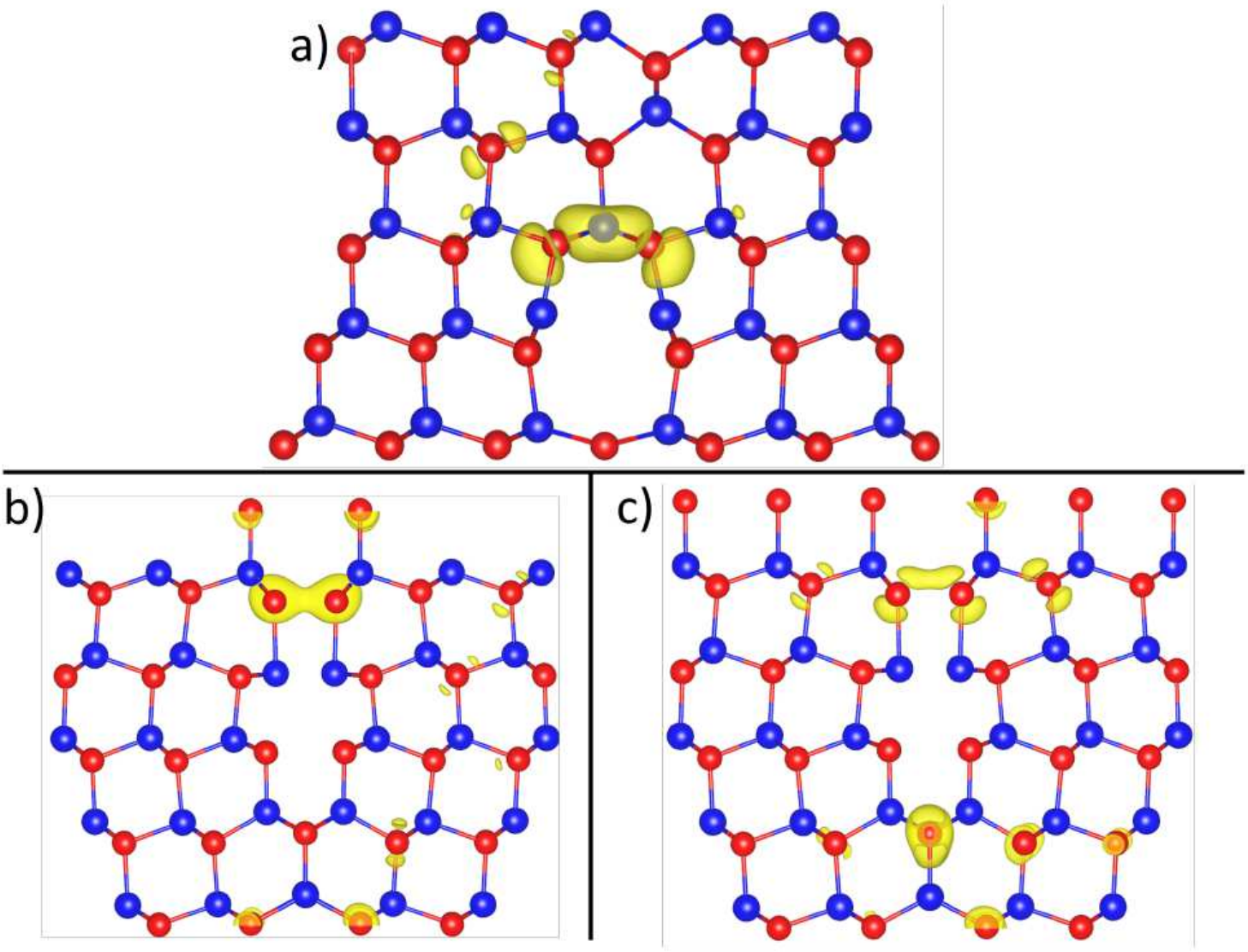

Figure 10

Partial Charges at the Grain Boundaries with a Stacking Fault Layer Present.(a) ‘Cross-boundary’ Te-Te interaction in the Cd-core responsible for the defect level at -0.6 eV in figure 9.(b) ‘Cross-boundary’ Te-Te interaction in the Te-core partially responsible for the defect level between -0.6 eV and 0 eV in figure 9. (c) Te defect caused by a non-standard Cd bond angle at the bottom of the Te-core partially responsible for the defect level between -0.6 eV and 0 eV in figure 9.